Lab on a Chip

ROYAL SOCIETY OF CHEMISTRY

PAPER

View Article Online
View Journal

Cite this: DOI: 10.1039/d6lc00016a

Multiphasic droplet microfluidics platform for controlled bacteria and mammalian cell co-culture

Ibraheem Alshareedah and Anand Kumar *

Microfluidics has revolutionized high-throughput miniaturized biological assays. However, co-culture of mammalian cells and bacteria remains challenging in microfluidic systems due to incompatible growth requirements, limited spatial control, and the requirement for a mammalian cell adhesion matrix. Here, we present a microfluidic platform that generates multiphasic droplets which encapsulate mammalian and bacterial cells, enabling their direct and indirect co-culture. By combining photopolymerizable hydrogels with polymer phase separation, we generate core–shell droplets composed of a liquid and a hydrogel compartment. The hydrogel compartment supports mammalian cell adhesion and culture, while the liquid compartment sustains bacterial growth. We demonstrate two droplet architectures that allow physical bacteria–mammalian cell contacts or enforce complete physical separation, representing direct and indirect co-culture. Our multiphasic droplets are stable, customizable, able to sustain co-culture for over 24 hours, and compatible with fluorescence-based cell sorting technologies. Overall, our multiphasic droplet microfluidic platform provides a scalable and versatile tool for high-throughput co-culture and screening of host–microbe interactions.

Received 7th January 2026,
Accepted 9th March 2026

DOI: 10.1039/d6lc00016a

rsc.li/loc

Introduction

Droplet microfluidics has shifted the paradigm of high-throughput biological assays, enabling millions of isolated micrometer-sized reaction vessels that can be quickly generated and accurately analyzed.[1–3] Such systems have transformed applications in single-cell sequencing,[4] antibody discovery,[5] and enzyme directed evolution studies[6] by providing precise control over sample volume, composition, and throughput.[3,4] Most cell biology-focused droplet microfluidic applications involve single cell analysis and spheroid/3D culture growth.[7–10] More advanced microfluidic platforms can now probe cell–cell interactions for mammalian cells or microbial communities.[11–15] However, studying the interactions of mammalian cells and bacteria with microdroplet-enabled control and throughput remains challenging. This is due to incompatible growth conditions, limited spatial organization, and the lack of complex droplet material properties that allow adherent mammalian cell culture while simultaneously supporting bacterial growth.

Current *in vitro* methods to study bacteria and host cell interactions rely on co-culturing both types of cells in the same media.[16,17] In general, the co-culture of different types of cells can be direct or indirect. Direct co-culture allows for physical contact between the interacting cells, while indirect co-culture utilizes a permeable physical barrier to prevent physical contact while allowing signaling and small molecule exchange.[18] While many co-culture models exist,[19] current techniques suffer from low throughput and limited scalability, making them poorly suited for large-scale interrogation of mammalian cell–bacteria interactions. Humans harbor more than 500 species of bacteria, few of which have been directly studied in the context of their influence on diseases such as *H. pylori* and *Fusobacterium*.[20,21] Furthermore, bacteria are adaptive, and their behavior depends on the composition of the entire bacterial population.[22] This presents multiple challenges to understanding the interplay between the bacteriome and host cells. Firstly, given the large number of bacteria that compose the bacteriome, high-throughput co-culture methods are needed to identify disease-relevant bacterial species. Secondly, given that bacteria can cooperate and compete, it is likely that disease-relevant phenotypes are affected not only by the presence of individual species but also by the presence of other species that may act synergistically to affect host cell behavior.[23] Thus, high-throughput screening pipelines that can identify phenotype-relevant bacterial species or communities are necessary to advance our understanding of the bacteriome–host cell interactions. To enable such pipelines, one must first develop methods that can co-culture bacteria and mammalian cells with high throughput. Droplet microfluidics provides a compelling route to develop high-throughput co-culture systems for mammalian cells and bacteria. Microdroplets are highly configurable and can be analyzed *via* sorting and sequencing

Microbial and Biome Sciences, Bioscience Division, Los Alamos National Laboratory, Los Alamos, New Mexico, USA. E-mail: akumar@lanl.gov

workflows.[8] However, current technologies face key limitations. Single-phase droplets can typically only be optimized for mammalian cells (by using hydrogels) or for bacteria (by using aqueous media).[24,25] A single-phase droplet that can culture both types of cells simultaneously is nearly impossible to develop, given the inherent differences between the two cell types. Furthermore, hydrogel materials that are often used for mammalian cell culture (such as agarose) are amenable to bacterial degradation. In addition, accurate positioning of both bacteria and mammalian cells within a co-culture vessel is essential since it dictates whether the co-culture is direct (allows physical interactions) or indirect (inhibits physical contacts). Given these limitations, a new droplet microfluidics platform is needed to allow sustainable, scalable, and controlled co-culture of mammalian cells and bacteria.

In this work, we use synthetic biocompatible polymers to create multiphasic microfluidic droplets (MMDs) with controlled architecture and non-uniform material properties. These MMDs can sustain both direct and indirect co-culture of mammalian cells and bacteria with high throughput. For direct co-culture, we demonstrate a one-step strategy that relies on liquid–liquid phase separation (LLPS) and photopolymerization to generate core–shell multiphasic droplets with a liquid core and a hydrogel shell. Bacteria are encapsulated in the liquid core while mammalian cells adhere to the liquid–gel interface, enabling direct co-culture of the two cell types. For indirect co-culture, we use an alternative strategy of sequential encapsulation of mammalian cells and bacteria that achieves complete engulfment of the host cells, inhibiting physical contact with bacterial cells. Importantly, both methods yield droplets small enough (<80 μm) to be sorted *via* conventional FACS sorting instruments using established protocols. This allows the integration with sorting and sequencing pipelines, enabling high-throughput study of bacteria and mammalian cell interactions. Overall, our platform harnesses physical principles to achieve both direct and indirect sustainable co-culture between mammalian cells and bacteria on a large scale, providing an avenue for accelerating large-scale studies of the complex interactions between host cells and bacterial populations.

Experimental

Mammalian cell culture

A549 cells were cultured in Gibco DMEM cell media supplemented with 10% FBS in a cell incubator at 37 °C and 5% CO_2. The cells were cultured in T25 flasks and passaged using TrypLE Express enzyme (for cell detachment) at 80% confluency. The number of live cells was counted using trypan blue dye and the Countess instrument to seed subsequent flasks or for use in encapsulation experiments. CellTracker RED CMTPX was used to stain the cells in fluorescence experiments. The staining process is done according to the manufacturer's protocol. Briefly, the CellTracker dye is diluted to ~4 μM using an FBS-free DMEM media and incubated with cells in suspension for 30 minutes at 37 °C. Cells are washed twice with PBS and resuspended in FBS-supplemented DMEM media for the remainder of the experiments.

Generation of green fluorescent *E. coli* Nissle 1917 (EcN) strain

The plasmid was derived from pGlo (BioRad), where we introduced an EcN native promoter PkatG that regulated the expression of a sfGFP reporter. The plasmid was transformed into in-house prepared EcN chemically competent cells. Transferred EcN colonies were grown on agar plates and stored at 4 °C. Bacteria were inoculated in LB broth and grown for 18 hours until an OD_{600} value of 0.6 was reached. Bacterial cells are then used for encapsulation experiments.

PEG–dextran phase separation assays

Norbornene-functionalized 4-arm polyethylene glycol was obtained from Creative PEGworks and used as received. PEG was resuspended in PBS at stock concentrations of 40% wt/vol (400 mg ml^{-1}). Dextran from *Leuconostoc* spp. (M.W. 400–600k) was purchased from Sigma Aldrich and reconstituted in PBS. PEG and dextran were mixed in a PBS-buffered solution at the desired concentration and then injected into a cell counting chamber (C-Slide, Nanoentek Inc.) before imaging on an EVOSM5000 microscope (FisherBrand).

PEG–dextran multiphasic microfluidic droplet generation

To generate multiphasic microfluidic droplets (MMDs), we first prepared solutions of 7–10% wt/vol of dextran and PEG in separate tubes. For fluorescence images, we added 5 μM of PEG-FITC (MW 2k, Sigma Aldrich) and dextran-Texas Red (MW 70k, Sigma Aldrich). The 1 mL solutions of dextran and PEG were then loaded on 1 mL Air-Tite Luer lock sterile syringes. The syringes were then connected to PTFE tubing, which is fed to a custom-made microfluidic chip (manufactured by uFluidix, Canada, see Fig. S1). Syringes were loaded on a Chemyx Fusion 4000× syringe pump. For the carrier oil, we used HFE7500 oil with 2% 008-Fluorosurfactant (RAN Biotechnologies, Inc) in a 5 mL Air-Tite Luer lock syringe loaded on Chemyx Fusion 200 syringe pump. The oil flow rate was set between 10 and 20 μL min^{-1}, and the PEG/dextran flow rates were set to 2/3 μL min^{-1}, respectively. Droplets were collected in a 2 mL Eppendorf tube containing 200 μL of mineral oil to prevent evaporation of the carrier oil. Ten microliters of droplet suspension were pipetted into a cell counting chamber slide (C-Slide, Nanoentek) and imaged using EVOS M5000 microscope equipped with DAPI, GFP, RFP, and Texas Red filter cubes.

PEG hydrogel mesh size determination

4-arm PEG norbornene (MW 20k) was mixed with thiol-PEG-thiol (MW 3400, Sigma Aldrich) and lithium phenyl-2,4,6-trimethylbenzoylphosphinate (LAP) photoinitiator to make a

photo-inducible PEG hydrogel. The final concentrations of the components were 10% 4-arm PEG-NB, 10 mM PEG-dithiol, and 0.1% (wt/vol) LAP. 1 μL of the gel precursor solution was sandwiched between a glass slide and a cover slip using Scotch double-sided tape. The gel precursor was then exposed to UV light for 60 seconds using AmScope LED-6 W-UV395 light illuminator set at medium intensity setting at a 6-inch distance. Following the photo-curing of PEG hydrogel, a solution of PBS and the desired probe (dextran-Texas Red of different sizes or BSA-FITC) was added to the imaging chamber using a pipette. All probe concentrations were approximately 10 μM. The chamber is then sealed from both ends with Loctite Super Glue Ultra Gel to prevent evaporation. The samples were immediately imaged using the EVOS M5000 microscope and then imaged again after 24 hours. Imaging was done away from the glass surface and at the hydrogel interface with the aqueous solution of probes.

Mammalian cell culture on PEG bulk hydrogels

Gel precursor solutions were prepared similarly to the mesh size experiment, except with different PEG concentrations. We prepared 10% PEG hydrogel using 10% 4-arm PEG-norbornene and 10 mM PEG-dithiol, as well as 5% PEG hydrogel using 5% 4-arm PEG and 5 mM PEG-dithiol. The LAP concentration in both gel precursor solutions was 0.1%. We also added 0.1 mM RGD peptide (GCGYGRGDSPG, GenScript) to promote cell adhesion to the hydrogel. RGD peptide binds to integrin receptors at the cell surface and has been shown to encourage cell growth in hydrogels.[26] All components were mixed in FBS-supplemented DMEM media. Cells were added at a concentration of 50 000 mL^{-1} to the hydrogel precursor solution. 100 μL of the hydrogel precursor cell suspension was placed in a 96-well plate and exposed to UV radiation at medium intensity (AmScope 6 Watt illuminator) at a distance of 5 inches for 60 seconds. After gel photocuring, 200 μL of FBS-supplemented DMEM media was added to each well, and the plate was kept in a cell culture incubator. The media was changed once on day 8 by pipetting. Hydrogels were imaged using EVOS M5000 by taking a 50-frame *Z*-stack that goes across the gel. The images shown in Fig. 3 are a summation *Z*-projection of the stacks that was done using Fiji ImageJ software.[27] The average diameter was measured using a custom Python script that performs Gaussian blurring and Otsu-thresholding before measuring diameters using region properties.

Encapsulation of bacteria and mammalian cells in MMDs *via* direct culture

The multiphasic microfluidic droplets were prepared as described previously. The 10% dextran solution was created with LB broth, and then 10 μL of 0.6 OD bacterial culture was added. The bacteria-laden dextran solution was loaded into a 1 mL syringe in the syringe pump described previously. For human cells, we added ~1–10 million cells per mL suspended in FBS-supplemented DMEM media along with 7–8% of 4-arm PEG-NB, 8 mM PEG-dithiol, 0.1% LAP, and 0.1 mM RGD. The cell-laden gel-precursor solution was loaded onto a syringe pump. Droplet generation (using the chip shown in Fig. S1a) and flow rates are the same as described in the multiphasic microfluidic droplet generation section. After droplet collection, the droplet suspension in HFE7500 oil was exposed to UV light at medium intensity at 5 inches away from the UV source (AmScope LED 395 nm 6 Watt illuminator). Droplets were imaged using the EVOS M5000 microscope and were kept at a cell incubator at 37 °C and 5% CO_2.

Cell viability in microfluidic droplets

Cells suspended in a gel-precursor medium containing 10% 4-arm PEG-norbornene, 10 mM PEG-dithiol, and 0.1% LAP. The medium contained 5 μM propidium iodide. Droplets were generated by running the cell-laden gel precursor solution in a microfluidic chip with a cross junction. The carrier phase is HFE7500 supplemented with 2% 008-Fluorosurfactant (RAN Biotechnologies, Inc.). After droplet generation, the droplets were cross-linked by exposing them to UV light for 60 seconds at low intensity. The droplet suspension is then placed in an open 1.5 mL centrifuge tube and topped with 200 μl of mineral oil to prevent evaporation. We found that droplets fuse and aggregate if the HFE7500 suspension is left in the air (data not shown). We believe this is due to changes in surfactant concentration at the air–HFE7500 interface that lead to droplet clumping/fusion. The tube is then placed in a cell culture incubator and covered with one layer of parafilm to further reduce evaporation. At each time point, 10 μL was drawn from the droplet suspension and pipetted into a cell counting slide that was subsequently imaged using EVOS M5000 microscope. For bacteria effects on cell viability, we performed the direct co-culture procedure to co-encapsulate *E. coli* cells with A549 cells as mentioned previously. Propidium iodide was added to stain dead cells. The fraction of viable cells was then counted manually by dividing the number of unstained cells (live) by the total cell count. Approximately 5 images containing more than 100 cells were analyzed.

Indirect co-culture *via* sequential encapsulation

Gel precursor solution containing 10% 8-arm PEG-NB (MW 10k, Creative PEGworks, 20 mM PEG-dithiol (MW 1k, Sigma Aldrich), 0.1% LAP, and 0.1 mM RGD. We also added A549 cells at a final concentration of 1–2 million cells per mL. Additionally, we added 1% BSA, 0.1% poloxamer 188 surfactant (Sigma-Aldrich), and 1 : 18 volume fraction of Optiprep density gradient solution (Sigma-Aldrich) to prevent cell sedimentation and clumping. The sample was injected into a microfluidic chip (see Fig. S1b) with a 20 μm nozzle. HFE7500 was injected into the oil channel. We used 8-arm PEG and a shorter PEG cross-linker to limit PEG hydrogel droplet swelling when they are transferred to water. The oil flow rate was set to 20 μL min^{-1}, and the sample flow rate was set to 2 μL min^{-1}. The resultant droplets were ~30 μM in diameter. After droplet

collection, droplets were cured using UV as described previously. To extract PEG hydrogel particles from oil, we added 20% (vol/vol) 1*H*,1*H*,2*H*,2*H*-perfluoro-1-octanol to the droplet suspension, which destabilizes the oil–water interface and results in all droplets sticking to each other and exiting the oil phase. The sample was then centrifuged at 4000*g* for 2 minutes, and the oil was discarded. The PEG-hydrogel particles were then resuspended in a PBS solution containing 0.1% poloxamer 188 with a pipette. The hydrogel particles were pelleted again using centrifugation and washed twice. At this stage, the hydrogel particle solution will still have small and empty oil droplets. Therefore, we pass the sample through a 10 μm pluriStrainer mini cell strainer and retrieve the hydrogel particles from the strainer.

To perform the re-encapsulation, we pellet the hydrogel particles and resuspend them in a solution containing a 50 : 50 mixture of LB broth and FBS-supplemented DMEM media, bacteria (*E. coli*) at an OD of 0.005 (100× dilution from 0.5 OD_{600} bacterial culture). The bacteria–hydrogel particle mixture was then fed into a microfluidic chip (Fig. S1b) with a larger nozzle of 40 μm. We use one flow rate for both the oil and the sample at 5–10 μL min^{-1} to produce larger droplets of ~60–70 μm. At this point, the hydrogel particles and bacteria are co-encapsulated stochastically. At high hydrogel particle concentration, we observe almost 100% encapsulation efficiency with a few droplets featuring two or three hydrogel particles within one droplet. The droplet suspension was then kept in a cell incubator for co-culture and imaged similarly to the other MMD samples.

Results

One-step generation of multiphasic droplets *via* aqueous two-phase systems

Aqueous two-phase systems (ATPS) are a class of mixtures that undergo segregative phase separation in which one phase concentrates one polymer and the other phase concentrates the other polymer.[28] The most famous and common ATPS system is the mixture of polyethylene glycol (PEG) and dextran.[29] These polymers come in a variety of molecular weights and are generally inert and non-toxic to cells.[30,31] When mixed at concentrations beyond the phase

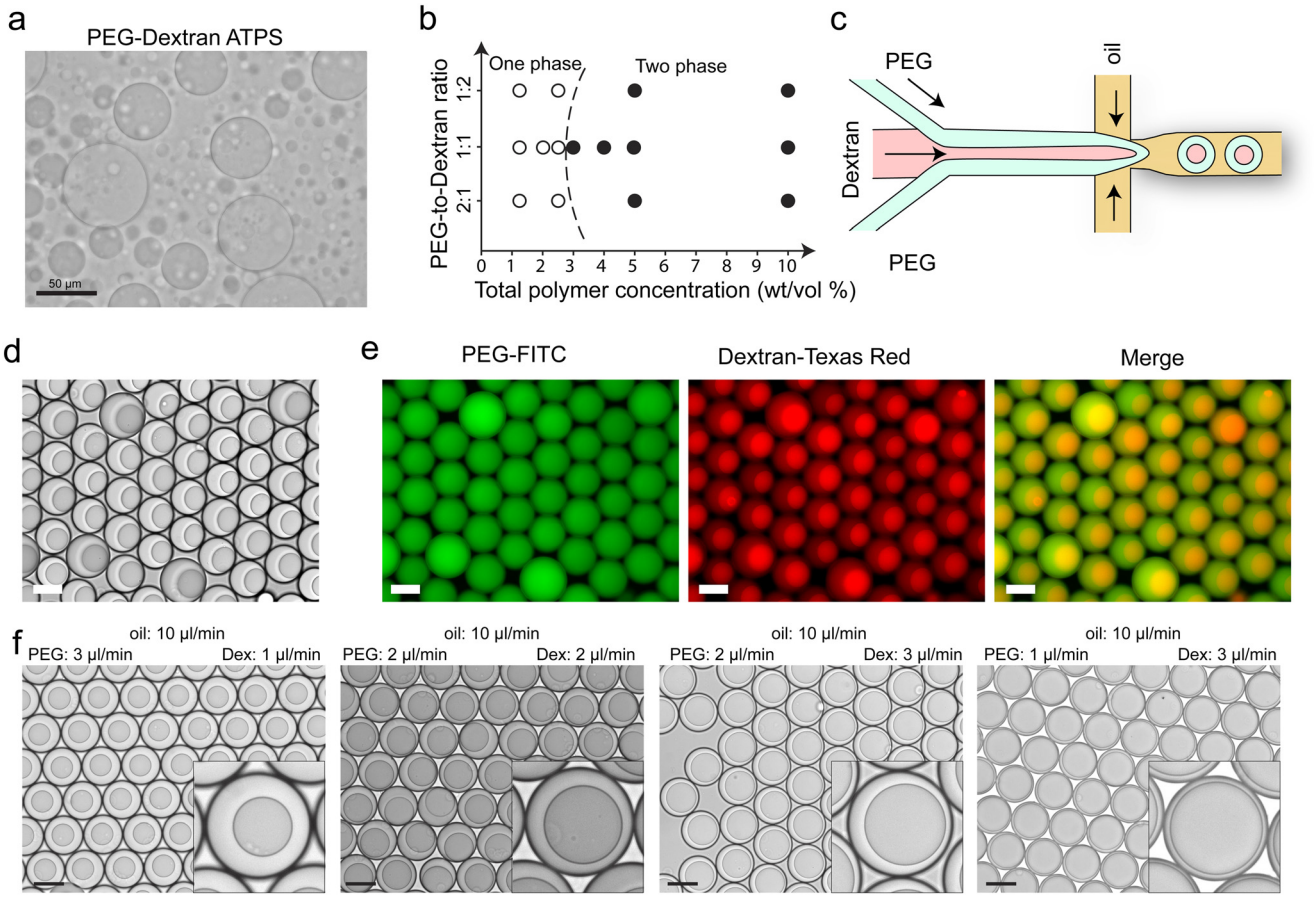

Fig. 1 A microfluidic platform to generate monodisperse multiphasic droplets. (a) Image of the phase separation of a mixture of PEG and dextran. (b) Phase diagram of PEG–DEX mixtures. (c) Diagram of the microfluidic device to create composite core–shell droplets. (d) Image of the microfluidic-generated multiphasic droplet suspension. (e) Fluorescence image showing the partition of both PEG and DEX molecules in MMDs. (f) Bright field images showing the change in multiphasic droplet structure upon changing the relative flow rates of the PEG and dextran phases in their respective channels. Inset shows zoomed-in images. Scale bars represent 50 μm.

separation threshold, these polymers undergo phase separation to form two phases, enriching PEG and dextran (Fig. 1a). By optimizing the mixing ratio and total polymer concentrations, the resulting phase volumes as well as their interface properties can be controlled. Since we are planning to culture adherent cells, a hydrogel is generally required for 3D cell culture.[32] Accordingly, we chose a 4-arm PEG polymer (MW 20k) and a linear dextran polymer (MW 500k). This system readily separates at concentrations around 3% wt/vol (Fig. 1b). We used a microfluidic chip that features a co-flow focusing design to mix dextran and PEG on chip to generate microfluidic droplets that are multiphasic (Fig. 1c and S1). At equal flow rates of 2 μl/minute, we observed the formation of monodisperse multiphasic core–shell droplets (Fig. 1d). Adding fluorescent PEG2K-FITC and dextran 70k–tetramethylrhodamine, we clearly see the unique composition of both phases (Fig. 1e). The dextran primarily concentrates in the core of the droplets while the small PEG probe seems to partition equally in the two phases (Fig. 1e). Additionally, changing the relative flow rates between dextran and PEG gives control over the volume of each compartment of the core–shell droplets (Fig. 1f).

PEG-based synthetic hydrogels for culturing human adherent cells

To enable the culture of mammalian adherent cells, a matrix needs to be present in the droplets.[33] Adherent cells do not grow in solution. Previous literature shows many examples of 3D cell culture grown in agarose, collagen, and PEG hydrogels.[33] Accordingly, we used norbornene-functionalized PEG polymers (10% wt/vol, MW 20k) combined with PEG-dithiol crosslinker as well as the integrin-binding RGD peptide[26,34] (Fig. 2a). The LAP photoinitiation is used to facilitate thiol-norbornene reaction upon UV light exposure. Following that, we tested diffusion across the hydrogel using dextran molecules of different sizes labeled with Texas Red. These probes were added to a hydrogel disk (Fig. 2b) after crosslinking and monitored using fluorescence microscopy. We found that dextran-3k (MW 3000) quickly diffused through the hydrogel interface (Fig. 3c), and within 24 hours, there was a significant concentration of the probe within the hydrogel (Fig. 2d). This indicates that the size of the dextran molecule is smaller than the mesh size of the hydrogel. Slower incorporation is observed in the case of dextran-10k (MW 10 000, Fig. 2c and d). Importantly, dextran-70k (MW 70 000) and BSA (MW ~67 000) showed minimal incorporation in the gel even after 24 hours (Fig. 2c and d). Given the reported hydrodynamic radii of dextran molecules,[35] we estimate the mesh size of the gel to range from 4–10 nm.

Next, we tested the suitability of our hydrogel formulation for mammalian cell culture of adherent cells. To that end, we prepared gel precursor solutions at 5% and 10% PEG concentration and suspended A549 cells within (Fig. 3a). The precursor solution was crosslinked on a 96-well plate and topped with cell culture growth media and placed in a cell incubator at 37 °C and 5% CO_2 (Fig. 3a). We found that 5% PEG hydrogel was more conducive to cell growth, evidenced by the observation of large spheroids (~100 μm in diameter) within 12 days of cell culture (Fig. 3b). Most spheroids observed grew from single cells as the initial cell density was relatively low (Fig. 3c). Conversely, with the same time window, the 10% PEG hydrogel did not show any growth (Fig. 3c), likely due to the excessive constraints placed on the cells by the higher density of polymers. Image analysis shows that the average size of the hydrogel-supported spheroids grows from <20 μm (single cell) to ~100 μm within 300 hours (~12 days, Fig. 3d). Accordingly, we concluded that ~5–10% PEG concentration in our system can support A549 cell culture.

Direct co-culture of bacteria and mammalian cells in multiphasic droplets

Since we established that LLPS can be harnessed to create core–shell microfluidic droplets and that PEG solutions can be functionalized to support mammalian cell culture, we sought to combine these two technologies to co-encapsulate bacteria and mammalian cells in multiphasic microfluidic droplets. We expect that human cells will adhere to the PEG–dextran interface due to the surface energy and will therefore be able to have direct but limited interactions with bacteria as compared to mixing the two types of cells.[36] Accordingly, we revised our microfluidics workflow to include a UV-induced polymerization step to polymerize the outer shell that is enriched with PEG-norbornene and add PEG dithiol crosslinkers as well as the photoinitiator (Fig. 4a). The photopolymerization did not alter the structure of our microdroplets (Fig. 4b). We then tested the ability of our MMDs to encapsulate each component separately. First, we cultured GFP-labeled *E. coli* to an OD of 0.6 and diluted it in the LB broth-supplemented dextran-rich phase at a final OD of 0.005. We then flowed bacteria-embedded dextran in the central channel of our microfluidic device and PEG hydrogel precursor solution into the shell channel to generate MMDs (Fig. 4c). After UV crosslinking and MMD collection, we found that *E. coli* were trapped in the dextran-rich core of the MMDs (Fig. 4d). Note that the encapsulation efficiency is controlled by Poisson distribution,[37] and the concentration of *E. coli* in the dextran phase dictates the distribution of the number of cells per droplet (Fig. S2). Methods that optimize the percentage of single cell encapsulation are described elsewhere in the literature.[38] We then incubated the droplet suspension in a 37 °C incubator and monitored bacterial growth within droplet cores using fluorescence microscopy. We found appreciable growth of bacterial colonies from a few *E. coli* cells over 27 hours of sample incubation (Fig. 4e and f). Importantly, our MMDs sustained *E. coli* growth up to 27 hours with no bursting of droplets or leaking into the PEG phase (Fig. 4e and f). This indicates

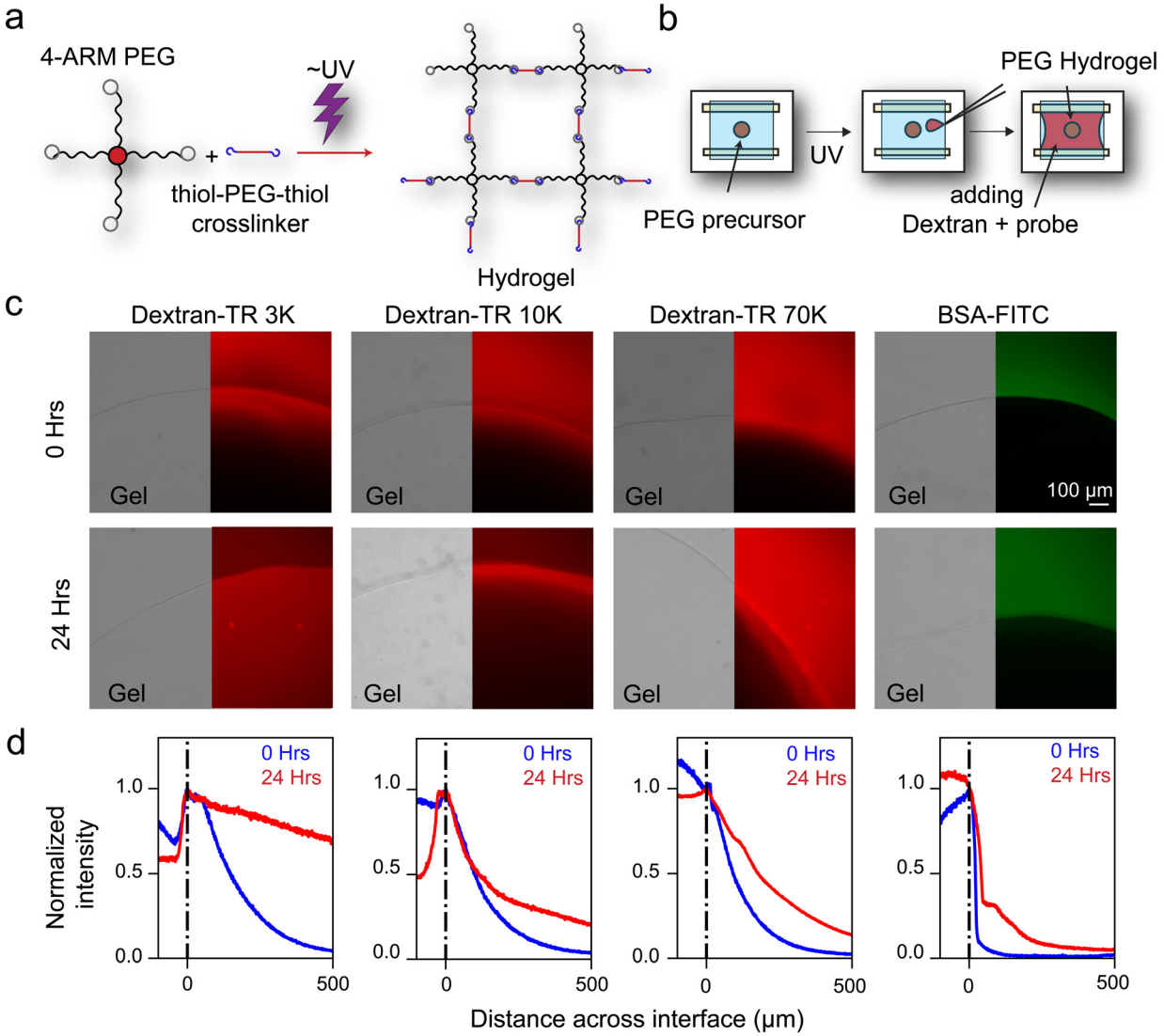

Fig. 2 Synthetic hydrogel system for culture of adherent cells. (a) Scheme of the chemical reaction used to create PEG hydrogels. (b) Diagram of the experiment to test the permeability of the PEG hydrogel. (c) Brightfield and fluorescence images of the penetration of fluorescent molecules into the PEG hydrogel over the course of 24 hours. (d) Plots showing the fluorescence intensity across the interface of the PEG hydrogel at different time points.

that the dextran phase is suitable as a carrier for *E. coli* culture within MMDs and that the PEG hydrogel is resistant to bacteria. Other systems, such as agarose gel particles, can withstand bacteria for a short period of time (~8 hours) before bacterial digestive enzymes degrade the hydrogel.[39] This highlights the utility of PEG-based hydrogel shells in sustaining bacterial culture.

Since our MMDs are designed as compartments that allow the co-culture of mammalian cells and bacteria, we next sought to encapsulate bacteria and mammalian cells simultaneously. To that end, we cultured A549 lung cancer cells, harvested them, and resuspended them in a gel precursor solution comprised of 4-arm PEG-norbornene, PEG dithiol, RGD peptide, and DMEM culture media. The final concentration of the cells was set to be ~5×10^6 cells per mL. We then flowed the cell-laden gel-precursor solution in the shell channel and the bacteria laden dextran solution in the core channel of our microfluidic chip (Fig. 4g). By controlling the flow rate of both channels, we were able to generate droplets of ~60 μm diameter (Fig. 4h). While most droplets contained bacteria, A549 cells were included in fewer droplets due to lower initial cell density (Fig. S3). Nevertheless, we were able to find many droplets that contain a single cell co-captured with a bacterial population of *E. coli* (Fig. 4h). There were also droplets featuring multiple cells trapped with an *E. coli* population (Fig. 4i). Notably, most A549 cells were observed to be attached to the PEG–dextran liquid–liquid interface (Fig. 4h and i and S3). This partitioning into the liquid–liquid interface has been reported previously in the literature and explained by the high interfacial energy in the PEG–dextran ATPS.[36,40] In our setup, we reason that such partitioning in the interface allows for both direct physical interactions with

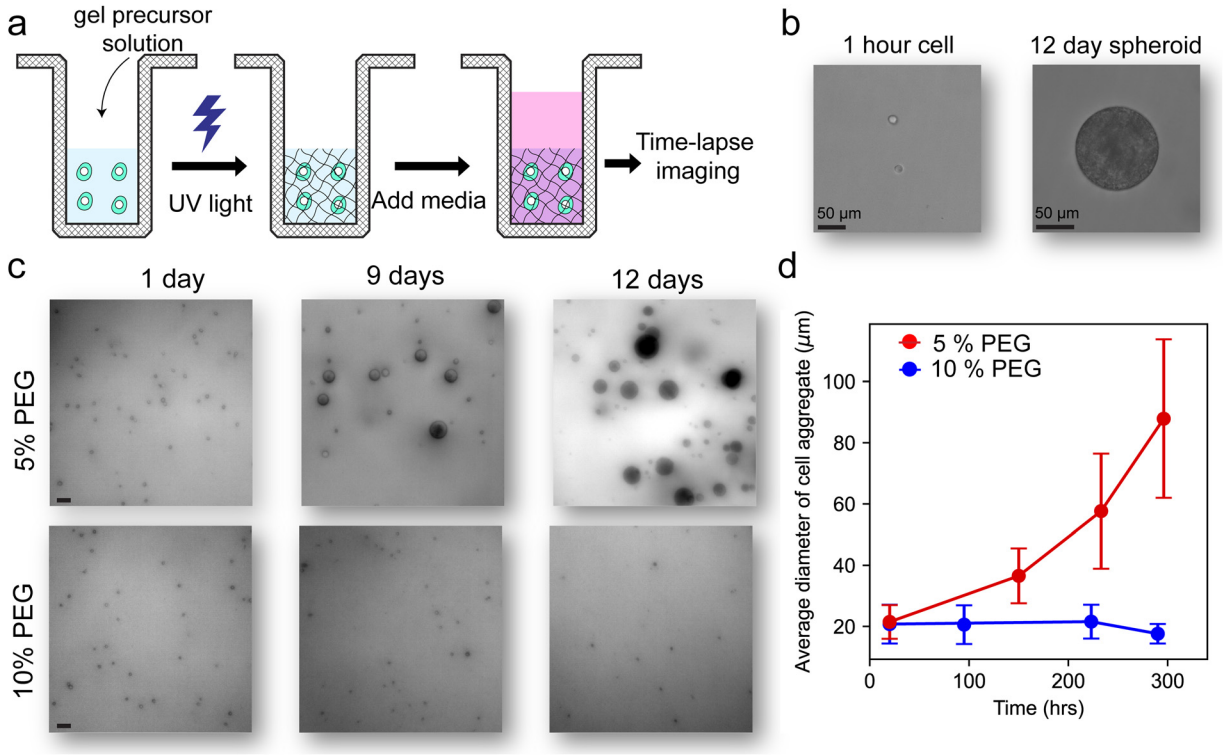

Fig. 3 Growth of A549 cells in PEG-based hydrogels. (a) Diagram of bulk gel cell growth experiment. (b) Growth of a single cell to a spheroid in 5% PEG hydrogel. (c) Time-lapse images of the evolution of A549 cells embedded in a PEG hydrogel of different concentrations. (d) Average diameter of spheroids in PEG hydrogel over time. Error bars represent the standard deviation. All scale bars are 50 μm.

bacteria as well as indirect physical interactions with bacteria through signaling molecules, while providing a template for cell adhesion.

In a separate experiment, we encapsulated mammalian cells in PEG hydrogels suspended in oil and added propidium iodide to monitor dead cells. Propidium iodide cannot penetrate live cell membranes and can only enter membrane-compromised dead cells.[41] Upon entering the cell, its fluorescence intensity increases by ~20-fold. We used propidium iodide to check cell viability in our microfluidic droplet system. For 50 μm diameter droplets, we found that cell viability is ~93% immediately after incubation (Fig. 4j and S4). After 24 hours of incubation, cell viability dropped to 70%. Within 48 hours of sample preparation, we found the cell viability fraction to drop significantly to 24% (Fig. 4j and S4). The drop in cell viability over time could be explained by the fact that droplets have limited nutrients available, metabolic wastes (*e.g.*, urea, CO_2, lactate, *etc.*) production, and oxygen depletion.[42] Note that the presence of our GFP-labeled *E. coli* did not affect the cell viability trend within microfluidic droplets when direct co-culture was used (Fig. S5). This could be specific to the particular strain used here (*E. coli* Nissle), which is a probiotic strain that has a positive effect on human cell viability.[43] Importantly, we used mineral oil to cover the HFE7500 carrier oil to prevent its evaporation. Mineral oil is known to be a poor medium for oxygen and carbon dioxide transport.[44] We hypothesized that increasing the droplet volume would likely enhance cell viability. Therefore, we repeated the cell viability experiment with larger droplets (~90 μm diameter) to confirm that nutrient availability plays a role in regulating cell viability. Indeed, after 48 hours, we found ~40% cell viability in cell-laden PEG hydrogels (Fig. 4j). This suggests that in order to preserve mammalian cell viability for longer co-culture, larger microfluidic droplets are needed.[42] This behavior is also known to be dependent on the cell type. While keeping droplets small enables droplet sorting using conventional FACS machines, larger droplets can support longer co-culture times. The limitation on droplet sorting could be mitigated by adopting newer sorting technologies such as fluorescence activated droplet sorting (FADS) systems.[45,46] Another avenue is further optimization of the system, which could potentially extend the viability window without needing to use large droplets by optimizing the buffer, media, and oxygen-permeable oils used during the incubation step.

Indirect co-culture of bacteria and human cells *via* sequential encapsulation

In many applications, studying indirect mammalian cell–bacteria interactions is equally important as direct physical interactions. Indirect interactions are carried out through signaling and metabolic pathways without the possibility of physical interactions between the cells. This is crucial as many *in vivo* systems do rely on indirect interactions.[47] For example, in the human gut, the human

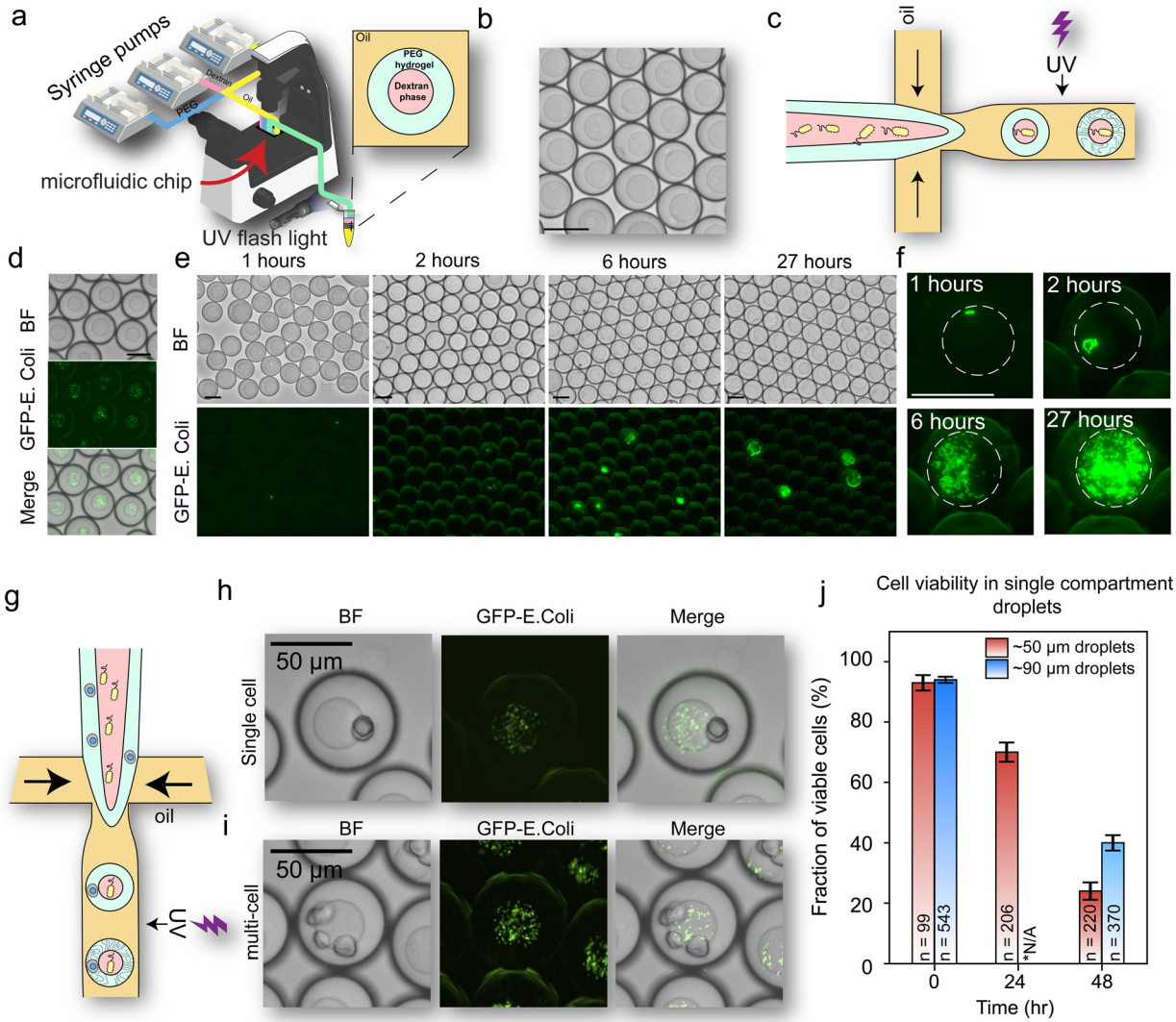

Fig. 4 Co-capture of mammalian cells and bacteria in multi-phasic droplets with a hydrogel shell. (a) Scheme of the experimental setup to create hydrogel MMDs. (b) Brightfield image of MMDs after UV-induced crosslinking. (c) Scheme of bacterial encapsulation in MMDs' core. (d) Brightfield and fluorescence images of GFP-labeled *E. coli* encapsulated in the core of MMDs. (e) Brightfield and fluorescence images of the growth of GFP-labeled *E. coli* in the core of MMDs for 27 hours. (f) Zoomed-in fluorescence images of bacterial colonies at 4 time points within MMDs. The white circle highlights the core of the MMD. (g) Scheme describing the co-encapsulation of bacteria and mammalian cells in MMDs' core and shell, respectively. (h) Brightfield and fluorescence images of a single cell encapsulated with bacteria in an MMD. (i) Same as (h) but with multi-cell encapsulation. (j) Cell viability plot for cells encapsulated in single-compartment hydrogel droplets of different diameters suspended in oil (see also Fig. S3).

bacteriome is separated from the epithelial lining of the stomach by the mucus membrane, which allows molecular exchange but prevents direct invasion of pathogens.[48] We therefore sought to test whether our microfluidic approach can offer fully separated reaction droplets for bacteria and mammalian cells as a microscale indirect co-culture method. To achieve indirect co-culture between mammalian cells and bacteria, we opted for a two-step procedure that relies on first embedding mammalian cells in PEG hydrogel without the presence of dextran (to eliminate the PEG–dextran interface, Fig. 5a). This, in principle, favors the PEG phase to completely engulf mammalian cells. After crosslinking the hydrogels, we transfer them to water containing a low concentration of bacteria (Fig. 5a). A re-encapsulation step ensures the formation of core–shell reaction droplets where the core contains embedded human cells and the shell harbors a bacterial population (Fig. 5a). To that end, we used an 8-arm PEG norbornene polymer with PEG1k-dithiol crosslinker. This system forms a stiffer gel than the previous system. Stiffer gels are necessary as PEG hydrogels are known to swell significantly when transferred to water.[49,50] To ensure that our final assemblies are smaller than 70 µm in diameter (compatible with FACS sorting), we set the flow rate of the first droplet generation step such that the produced particles have a diameter of ~35 µm (Fig. S6). After transferring the hydrogel particles to water, our particles swelled to a

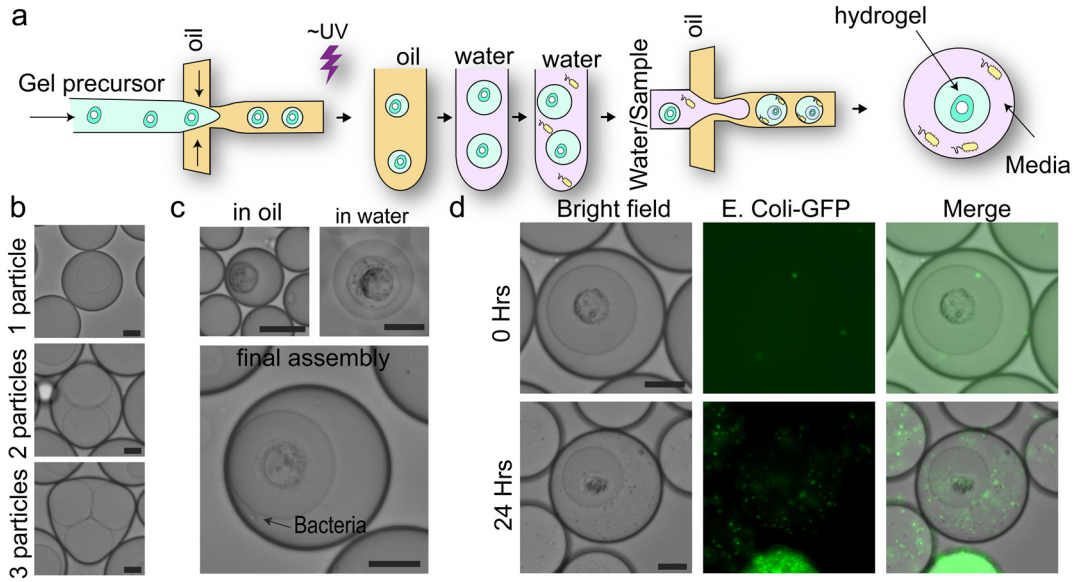

Fig. 5 A two-step microfluidic approach to generate reaction droplets for indirect co-culture of mammalian cells and bacteria. (a) Scheme of the two-step experimental protocol to create hydrogel MMDs. (b) Encapsulated hydrogel particles in aqueous droplets with single particle, double particle, and triple particle encapsulation. (c) Brightfield images of A549 cells encapsulated at the center of the PEG hydrogel in oil, in water, and then re-encapsulated in a fully assembled MMD with bacteria in the shell. (d) Bright field and fluorescent images of A549 cells and GFP-labeled *E. coli* encapsulated in MMDs for 0 and 24 hours using the sequential encapsulation method. All scale bars are 20 μm.

diameter of ~45 μm (Fig. S6). Next, we reintroduced the water-based hydrogel particle suspension to a microfluidic device and adjusted the flow rate such that we mostly encapsulate one hydrogel particle per droplet (Fig. 5b) and that our final multi-compartment droplet had a diameter of ~70 μm. We also observed double and triple encapsulations depending on the chosen flow rates (Fig. 5b). We then repeated the process but now adding A549 cells to the PEG precursor solution along with DMEM growth media to test for complete cell encapsulation. We found that most cells were positioned within the droplets and away from the PEG–oil interface initially (Fig. 5c). Upon crosslinking and rehydrating the hydrogel particles, most cells remained within the core of the hydrogel particles and away from the interface (Fig. 5c). Next, we added *E. coli* to the aqueous carrier phase of the hydrogel suspension and re-introduced it to a microfluidic droplet generator. As a result, we produced core–shell multiphasic droplets that include both bacteria in the shell and mammalian cells in the core and away from the interface (Fig. 5c). This procedure, therefore, allows us to generate MMDs that support indirect co-culture between bacteria and mammalian cells. Importantly, these composite droplets were able to sustain both mammalian cells and bacteria for 24 hours (Fig. 5d).

Discussion and conclusion

In this work, we present a multiphasic droplet microfluidic platform that addresses central limitations in droplet-based co-culture systems: the lack of control over spatial organization, material properties, and co-culture interaction modes. While these limitations may be addressed separately in other works in the literature, our platform solves these problems simultaneously by providing independent control over the droplet compartment properties and cell partitioning within. This enables co-culturing cells with different environmental culture requirements, such as bacteria and mammalian/human cells. Using a combination of polymer phase separation and photopolymerizable synthetic hydrogels, we generate uniform core–shell droplets that recruit mammalian cells and bacteria in different compartments with distinct chemical and material properties. This droplet structure facilitates co-culture for over 24 hours and is compatible with fluorescence-based droplet analysis and sorting workflows, allowing for a scalable microfluidic framework for controlled co-culture.

Multiphasic droplets have been reported previously *via* a plethora of microfluidic strategies, including double emulsions,[51] particle templates,[52] and aqueous two-phase systems.[53] However, most existing platforms can be used for either mammalian cells or bacteria, but not both. In addition, single-phase droplets lack the material properties required to support adherent cell culture, while hydrogel-based droplets, such as agarose, can be susceptible to bacterial degradation and can slow down bacterial growth.[54] Contrastingly, the synthetic PEG-based hydrogel provides a stable support to mammalian co-culture while possessing the necessary features to achieve phase separation with dextran, enabling a hybrid liquid–gel composite droplet architecture. This has enabled reproducible and spontaneous generation of core–shell droplets with non-uniform material properties, sustaining both mammalian cell adhesion and an aqueous

environment for bacterial growth. Notably, this is done without complex device architectures.

The presented platform offers a distinctive feature in the ability to switch between direct and indirect co-culture through architectural control. In the one-step encapsulation, mammalian cells adhere to the liquid–gel interface and can have physical contact with the bacteria that are concentrated in the liquid core of the droplet. In contrast, sequential encapsulation results in full separation between mammalian cells and bacteria, permitting only indirect interactions through metabolites and small molecules. This decoupling of physical and biochemical interactions provides a droplet-based analogue to conventional direct *versus* indirect co-culture methods with the added benefits of high-throughput, precise spatial control, and low material volumes.

The relevance of these different modes of co-culture is underscored by the fact that host-microbiome biology depends on the environmental context. In humans and other mammals, the majority of the complex bacterial population does not physically interact with epithelial cells, as these layers of cells are covered with a permeable mucus barrier.[48] Hence, most host–bacteria interactions occur *via* signaling molecules and metabolites (indirect co-culture, Fig. 6a). Severe chronic conditions occur when the mucus barrier is damaged, and bacteria can access the epithelial cells physically (direct co-culture).[55,56] Even then, the cells that are exposed to bacteria are the interface cells in most cases, where they only "see" bacteria from one direction and are surrounded by other materials or cells in the other directions. Therefore, host–bacteria interactions are more appropriately studied when the host cell is either shielded physically from bacteria by a permeable matrix (Fig. 6a) or if they are at an interface that exposes them to a bacterial suspension while preserving adhesion to a matrix (Fig. 6b). Our microfluidic platform allows the study of these two scenarios in one platform, enabling systematic investigation of how spatial constraints affect bacterial influence on host cells. This is particularly relevant as bacteria comprise the largest biomass of the human microbiome and are intimately connected to disease conditions.[23,57–59]

As with all droplet-based platforms, there are trade-offs between droplet size, culture duration, and downstream compatibility. Smaller droplets can be processed for sorting using conventional flow cytometry.[15,60] However, they impose constraints on cell viability due to nutrient availability, waste accumulation, and the transport of oxygen.[42] Larger droplets are more suited for longer cell cultures; however, they pose a challenge with conventional flow cytometers and can only be sorted with alternative techniques such as dielectric droplet sorting.[45] With that said, further optimization remains possible through culture media formulation, carrier oil

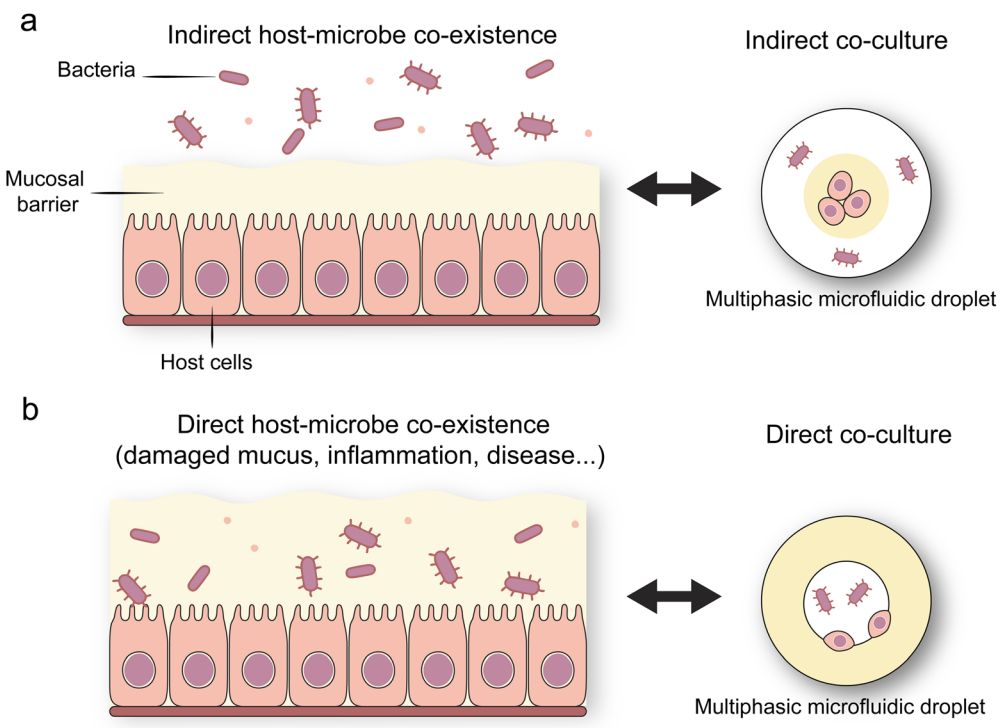

Fig. 6 Direct and indirect co-culture methods for different biological conditions. (a) Schematic diagram of host cells in the epithelial lining separated from the gut bacteriome through a mucus barrier. This is the case of a healthy gut and is represented by an indirect co-culture experiment where physical contacts between bacteria and host cells are absent. (b) Same as (a) but for the case of damaged mucus, where bacteria and human cells can interact physically as well as biochemically. In such cases, a direct co-culture experiment is more appropriate to represent host–bacteria interactions.

oxygen transport properties, and droplet size control based on the application at hand.

In sum, we show that phase separation combined with microfluidics facilitates the creation of multiphasic microfluidic droplets that support direct and indirect co-culture of bacteria and mammalian cells at high throughput. Our miniaturized droplet co-culture vessels provide precise control over cell localization, bacteria–host interaction modes, and molecular exchange through integrating liquid and hydrogel compartments within a single droplet. While microfluidic droplet limitations exist and can be further optimized, the presented platform establishes a versatile microfluidic architecture for high-throughput co-culture and screening applications. This approach expands the design space for droplet-based co-culture, potentiating new tools for high-throughput interrogation of bacteria–mammalian cell interactions.

Conflicts of interest

The authors declare that an invention disclosure related to this work has been filed with their institution.

Data availability

All data relevant to the conclusions of this manuscript are presented in the main text and supplementary information. All data are available from the authors upon reasonable request.

Supplementary information (SI) is available. See DOI: https://doi.org/10.1039/d6lc00016a.

Acknowledgements

The authors would like to acknowledge Katelyn Green, Sang-Min Shin, and Ramesh Jha (R. J.) for providing the GFP-labeled *E. coli* Nissle strain, which was generated as part of other ongoing research supported by an internal grant from Los Alamos National Laboratory (LANL), specifically the Laboratory Directed Research and Development (LDRD) program (0240803ER: A Living Diagnostic-Therapeutic System), awarded to R. J. and A. K. This work is supported by the LANL Frederick Reines Fellowship (LDRD 20251143PRD1) awarded to I. A. The authors also acknowledge Jason Patrick Martinez at the Innovation Hub and Elisa Wasson, a scientist in the Biochemistry and Biotechnology Group, Bioscience Division, LANL, for providing microfluidics-related supplies.

References

1 S. Mashaghi, *et al.*, Droplet microfluidics: A tool for biology, chemistry and nanotechnology, *TrAC, Trends Anal. Chem.*, 2016, **82**, 118–125.
2 Z. Chen, *et al.*, Trends in droplet microfluidics: From droplet generation to biomedical applications, *Langmuir*, 2022, **38**(20), 6233–6248.
3 M. T. Guo, *et al.*, Droplet microfluidics for high-throughput biological assays, *Lab Chip*, 2012, **12**(12), 2146–2155.
4 W.-m. Zhou, *et al.*, Microfluidics applications for high-throughput single cell sequencing, *J. Nanobiotechnol.*, 2021, **19**(1), 312.
5 A. Gérard, *et al.*, High-throughput single-cell activity-based screening and sequencing of antibodies using droplet microfluidics, *Nat. Biotechnol.*, 2020, **38**(6), 715–721.
6 A. Fallah-Araghi, *et al.*, A completely in vitro ultrahigh-throughput droplet-based microfluidic screening system for protein engineering and directed evolution, *Lab Chip*, 2012, **12**(5), 882–891.
7 H. N. Joensson and H. Andersson Svahn, Droplet microfluidics—A tool for single-cell analysis, *Angew. Chem., Int. Ed.*, 2012, **51**(49), 12176–12192.
8 K. Matuła, F. Rivello and W. T. Huck, Single-cell analysis using droplet microfluidics, *Adv. Biosyst.*, 2020, **4**(1), 1900188.
9 Y. Wang, *et al.*, Recent methods of droplet microfluidics and their applications in spheroids and organoids, *Lab Chip*, 2023, **23**(5), 1080–1096.
10 L. Yu, M. C. Chen and K. C. Cheung, Droplet-based microfluidic system for multicellular tumor spheroid formation and anticancer drug testing, *Lab Chip*, 2010, **10**(18), 2424–2432.
11 J. L. Madrigal, *et al.*, Characterizing cell interactions at scale with made-to-order droplet ensembles (MODEs), *Proc. Natl. Acad. Sci. U. S. A.*, 2022, **119**(5), e2110867119.
12 Q. Chen, *et al.*, Controlled assembly of heterotypic cells in a core–shell scaffold: organ in a droplet, *Lab Chip*, 2016, **16**(8), 1346–1349.
13 R. H. Hsu, *et al.*, Microbial interaction network inference in microfluidic droplets, *Cell Syst.*, 2019, **9**(3), 229–242.e4.
14 J. Ohan, *et al.*, High-throughput phenotyping of cell-to-cell interactions in gel microdroplet pico-cultures, *BioTechniques*, 2019, **66**(5), 218–224.
15 Y. Ding, *et al.*, Robust double emulsions for multicolor fluorescence-activated cell sorting, *Anal. Chem.*, 2024, **96**(37), 14809–14818.
16 S. E. Mountcastle, *et al.*, A review of co-culture models to study the oral microenvironment and disease, *J. Oral Microbiol.*, 2020, **12**(1), 1773122.
17 Y. Qi, *et al.*, In vitro models to study human gut-microbiota interactions: Applications, advances, and limitations, *Microbiol. Res.*, 2023, **270**, 127336.
18 M. A. Vis, K. Ito and S. Hofmann, Impact of culture medium on cellular interactions in in vitro co-culture systems, *Front. Bioeng. Biotechnol.*, 2020, **8**, 911.
19 R. Kim, Advanced organotypic in vitro model systems for host–microbial coculture, *BioChip J.*, 2023, **17**(2), 147–173.
20 E. McIlvanna, *et al.*, Fusobacterium nucleatum and oral cancer: a critical review, *BMC Cancer*, 2021, **21**(1), 1212.
21 M. Alipour, Molecular mechanism of Helicobacter pylori-induced gastric cancer, *J. Gastrointest. Cancer*, 2021, **52**, 23–30.

22 R. D. Prescott and A. W. Decho, Flexibility and adaptability of quorum sensing in nature, *Trends Microbiol.*, 2020, **28**(6), 436–444.
23 G. El Tekle and W. S. Garrett, Bacteria in cancer initiation, promotion and progression, *Nat. Rev. Cancer*, 2023, **23**(9), 600–618.
24 H. Huang, *et al.*, Generation and manipulation of hydrogel microcapsules by droplet-based microfluidics for mammalian cell culture, *Lab Chip*, 2017, **17**(11), 1913–1932.
25 A. M. Kaushik, *et al.*, Accelerating bacterial growth detection and antimicrobial susceptibility assessment in integrated picoliter droplet platform, *Biosens. Bioelectron.*, 2017, **97**, 260–266.
26 F. Yang, *et al.*, The effect of incorporating RGD adhesive peptide in polyethylene glycol diacrylate hydrogel on osteogenesis of bone marrow stromal cells, *Biomaterials*, 2005, **26**(30), 5991–5998.
27 J. Schindelin, *et al.*, Fiji: an open-source platform for biological-image analysis, *Nat. Methods*, 2012, **9**(7), 676–682.
28 M. Iqbal, *et al.*, Aqueous two-phase system (ATPS): an overview and advances in its applications, *Biol. Proced. Online*, 2016, **18**(1), 18.
29 M. W. Edelman, E. Van Der Linden and R. H. Tromp, Phase separation of aqueous mixtures of poly (ethylene oxide) and dextran, *Macromolecules*, 2003, **36**(20), 7783–7790.
30 J. Cadée, *et al.*, In vivo biocompatibility of dextran-based hydrogels, *J. Biomed. Mater. Res.*, 2000, **50**(3), 397–404.
31 K. Bjugstad, *et al.*, Biocompatibility of PEG-based hydrogels in primate brain, *Cell Transplant.*, 2008, **17**(4), 409–415.
32 M. W. Tibbitt and K. S. Anseth, Hydrogels as extracellular matrix mimics for 3D cell culture, *Biotechnol. Bioeng.*, 2009, **103**(4), 655–663.
33 F. Ruedinger, *et al.*, Hydrogels for 3D mammalian cell culture: a starting guide for laboratory practice, *Appl. Microbiol. Biotechnol.*, 2015, **99**(2), 623–636.
34 Z. Jiang, *et al.*, A microfluidic-based cell encapsulation platform to achieve high long-term cell viability in photopolymerized PEGNB hydrogel microspheres, *J. Mater. Chem. B*, 2017, **5**(1), 173–180.
35 J. K. Armstrong, *et al.*, The hydrodynamic radii of macromolecules and their effect on red blood cell aggregation, *Biophys. J.*, 2004, **87**(6), 4259–4270.
36 J. P. Frampton, *et al.*, Rapid Self-Assembly of Macroscale Tissue Constructs at Biphasic Aqueous Interfaces, *Adv. Funct. Mater.*, 2015, **25**(11), 1694–1699.
37 T. Tang, *et al.*, Enhancing single-cell encapsulation in droplet microfluidics with fine-tunable on-chip sample enrichment, *Microsyst. Nanoeng.*, 2024, **10**(1), 3.
38 D. J. Collins, *et al.*, The Poisson distribution and beyond: methods for microfluidic droplet production and single cell encapsulation, *Lab Chip*, 2015, **15**(17), 3439–3459.
39 Y.-J. Eun, *et al.*, Encapsulating bacteria in agarose microparticles using microfluidics for high-throughput cell analysis and isolation, *ACS Chem. Biol.*, 2011, **6**(3), 260–266.
40 C. Han, S. Takayama and J. Park, Formation and manipulation of cell spheroids using a density adjusted PEG/DEX aqueous two phase system, *Sci. Rep.*, 2015, **5**(1), 11891.
41 C. Riccardi and I. Nicoletti, Analysis of apoptosis by propidium iodide staining and flow cytometry, *Nat. Protoc.*, 2006, **1**(3), 1458–1461.
42 S. Sart, *et al.*, Cell culture in microfluidic droplets, *Chem. Rev.*, 2022, **122**(7), 7061–7096.
43 H. Wang, *et al.*, Escherichia coli Nissle 1917-derived factors reduce cell death and late apoptosis and increase transepithelial electrical resistance in a model of 5-fluorouracil-induced intestinal epithelial cell damage, *Cancer Biol. Ther.*, 2014, **15**(5), 560–569.
44 L. S. Kubie, The solubility of o2, co2, and n2 in mineral oil and the transfer of carbon dioxide from oil to air, *J. Biol. Chem.*, 1927, **72**(2), 545–548.
45 J.-C. Baret, *et al.*, Fluorescence-activated droplet sorting (FADS): efficient microfluidic cell sorting based on enzymatic activity, *Lab Chip*, 2009, **9**(13), 1850–1858.
46 H.-D. Xi, *et al.*, Active droplet sorting in microfluidics: a review, *Lab Chip*, 2017, **17**(5), 751–771.
47 J. K. Nicholson, *et al.*, Host-gut microbiota metabolic interactions, *Science*, 2012, **336**(6086), 1262–1267.
48 S. Cornick, A. Tawiah and K. Chadee, Roles and regulation of the mucus barrier in the gut, *Tissue Barriers*, 2015, **3**(1–2), e982426.
49 Q. T. Nguyen, *et al.*, Cartilage-like mechanical properties of poly (ethylene glycol)-diacrylate hydrogels, *Biomaterials*, 2012, **33**(28), 6682–6690.
50 Y. Song, *et al.*, Mechanically and Chemically Defined PEG Hydrogels Improve Reproducibility in Human Cardioid Development, *Adv. Healthcare Mater.*, 2025, **14**(16), 2403997.
51 T. Nisisako, S. Okushima and T. Torii, Controlled formulation of monodisperse double emulsions in a multiple-phase microfluidic system, *Soft Matter*, 2005, **1**(1), 23–27.
52 D. J. Sukovich, *et al.*, Bulk double emulsification for flow cytometric analysis of microfluidic droplets, *Analyst*, 2017, **142**(24), 4618–4622.
53 C. D. Crowe and C. D. Keating, Microfluidic control of coexisting chemical microenvironments within multiphase water-in-fluorocarbon droplets, *Langmuir*, 2022, **38**(5), 1811–1820.
54 N. Kandemir, *et al.*, Mechanical interactions between bacteria and hydrogels, *Sci. Rep.*, 2018, **8**(1), 10893.
55 J. E. Fishman, *et al.*, The intestinal mucus layer is a critical component of the gut barrier that is damaged during acute pancreatitis, *Shock*, 2014, **42**(3), 264–270.
56 C. T. Capaldo, D. N. Powell and D. Kalman, Layered defense: how mucus and tight junctions seal the intestinal barrier, *J. Mol. Med.*, 2017, **95**(9), 927–934.
57 R. Sender, S. Fuchs and R. Milo, Revised estimates for the number of human and bacteria cells in the body, *PLoS Biol.*, 2016, **14**(8), e1002533.
58 S. Menees and W. Chey, The gut microbiome and irritable bowel syndrome, *F1000Research*, 2018, **7**(F1000 Faculty Rev), 1029.

59 A. Zaky, *et al.*, The role of the gut microbiome in diabetes and obesity-related kidney disease, *Int. J. Mol. Sci.*, 2021, **22**(17), 9641.

60 M. Hai, *et al.*, Flow cytometry: a new method to investigate the properties of water-in-oil-in-water emulsions, *Langmuir*, 2004, **20**(6), 2081–2085.